### **ORIGINAL ARTICLE**



# Evolutionary scaling and cognitive correlates of primate frontal cortex microstructure

Cheryl D. Stimpson<sup>1,2,3</sup> · Jeroen B. Smaers<sup>4</sup> · Mary Ann Raghanti<sup>5</sup> · Kimberley A. Phillips<sup>6,7</sup> · Bob Jacobs<sup>8</sup> · William D. Hopkins<sup>9</sup> · Patrick R. Hof<sup>10</sup> · Chet C. Sherwood<sup>1</sup>

Received: 2 July 2023 / Accepted: 2 October 2023 / Published online: 27 October 2023 © The Author(s), under exclusive licence to Springer-Verlag GmbH Germany, part of Springer Nature 2023

### **Abstract**

Investigating evolutionary changes in frontal cortex microstructure is crucial to understanding how modifications of neuron and axon distributions contribute to phylogenetic variation in cognition. In the present study, we characterized microstructural components of dorsolateral prefrontal cortex, orbitofrontal cortex, and primary motor cortex from 14 primate species using measurements of neuropil fraction and immunohistochemical markers for fast-spiking inhibitory interneurons, large pyramidal projection neuron subtypes, serotonergic innervation, and dopaminergic innervation. Results revealed that the rate of evolutionary change was similar across these microstructural variables, except for neuropil fraction, which evolves more slowly and displays the strongest correlation with brain size. We also found that neuropil fraction in orbitofrontal cortex layers V–VI was associated with cross-species variation in performance on experimental tasks that measure self-control. These findings provide insight into the evolutionary reorganization of the primate frontal cortex in relation to brain size scaling and its association with cognitive processes.

**Keywords** Brain evolution · Neuropil · Serotonin · Dopamine · Parvalbumin · Interneuron

# Introduction

The frontal cortex is centrally involved with motor planning and cognitive functions, such as decision making, goal-directed behavior, working memory, and attentional control (Passingham and Lau 2022). In primate brain evolution, granular prefrontal cortex regions, defined by reciprocal connections with the dorsomedial thalamus (Berger et al. 1991),

have become further specialized (Aboitiz and Garcia 1997; Berger et al. 1991; Carmichael and Price 1994; Goldman-Rakic 1988; Kass 2013; Passingham and Wise 2012; Preuss and Goldman-Rakic 1991; Smaers et al. 2017). Haplorhine primates (i.e., tarsiers, monkeys, apes, and humans) display additional areas of dorsomedial, mid-lateral, and ventral prefrontal cortex compared to strepsirrhines (i.e., lemurs, galagos, pottos, and lorises), suggesting that neuroanatomical

- ☐ Chet C. Sherwood sherwood@gwu.edu
- Department of Anthropology and Center for the Advanced Study of Human Paleobiology, The George Washington University, Washington, DC, USA
- DoD/USU Brain Tissue Repository and Neuropathology Program, Uniformed Services University (USU), Bethesda, MD, USA
- <sup>3</sup> Henry M. Jackson Foundation for the Advancement of Military Medicine, Inc, Bethesda, MD, USA
- Department of Anthropology, Stony Brook University, Stony Brook, NY, USA
- Department of Anthropology and School of Biomedical Sciences, Kent State University, Kent, OH, USA

- Department of Psychology, Trinity University, San Antonio, TX, USA
- Southwest National Primate Research Center, Texas Biomedical Research Institute, San Antonio, TX, USA
- Department of Psychology, Laboratory of Quantitative Neuromorphology, Colorado College, Colorado Springs, CO, USA
- Department of Comparative Medicine, Michale E Keeling Center for Comparative Medicine and Research, M D Anderson Cancer Center, Bastrop, TX, USA
- Nash Family Department of Neuroscience, Center for Discovery and Innovation, and Friedman Brain Institute, Icahn School of Medicine at Mount Sinai, New York, NY, USA

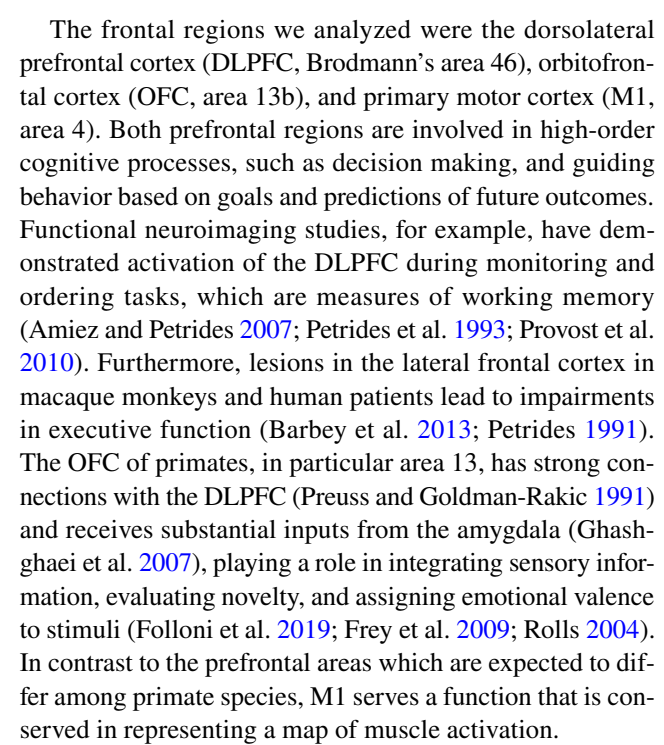


modifications and accompanying behavioral adaptations associated with these regions have been important in primate diversification (Preuss and Goldman-Rakic 1991; Sallet et al. 2013). Ventromedial prefrontal cortex is particularly important for emotional regulation and guidance of social interaction (Rolls 2004).

Differences among primate species have been reported in cytoarchitecture, pyramidal neuron morphology, cell type composition, neurotransmitter-expressing axon densities, and other aspects of histological architecture in frontal cortex regions (Bianchi et al. 2013; Elston et al. 2011; Herculano-Houzel et al. 2007; Jacobs et al. 2018; Semendeferi et al. 2011; Raghanti et al. 2008a, b; Sherwood et al. 2004; Spocter et al. 2012). To date, however, there has not yet been a comprehensive analysis that models evolutionary changes concurrently in various features of cortical microstructure across different regions and layers. The aim of the current study was to generate a comparative dataset characterizing frontal cortex microstructure from diverse primate species to identify evolutionary shifts and scaling patterns in a phylogenetic framework.

Microstructural elements such as serotonergic and dopaminergic innervation, local inhibitory interneurons, and long-range projection neurons all play important roles in shaping the function of the cerebral cortex. Serotonin and dopamine are key neurotransmitters that modulate prefrontal cortex activity, with serotonin regulating mood and attention, and dopamine modulating motivation and reward processing (Cools and Arnsten 2022). Local inhibitory interneurons regulate the activity of nearby neurons, controlling their spiking dynamics and information encoding (Fishell and Kepecs 2020). Long-range projection neurons connect different regions of the brain, participating in signal integration and high-order cognitive processing (Charvet 2023; Hilgetag et al. 2019). The interplay among these different systems has likely played a crucial role in the development of prefrontal cortex function in primates, which is critical for complex cognitive abilities such as decision-making, working memory, and executive function (Preuss and Wise 2022).

In 14 species of primates, we employed immunohistochemical markers for fast-spiking GABAergic inhibitory interneurons (parvalbumin, PV), large pyramidal neuron subtypes involved in corticocortical connectivity (non-phosphorylated neurofilament H, NEFH), serotonergic innervation (serotonin transporter, SERT), and dopaminergic innervation (tyrosine hydroxylase, TH) (Campbell et al. 1989; Carmichael and Price 1994; Gabbott and Bacon 1996; Gabbott et al. 1997; Hof and Sherwood 2005; Hof et al. 1995a, 1995b; Raghanti et al. 2008a, b; Sherwood et al. 2004, 2007; Stimpson et al. 2016; Wendland et al. 2005). Additionally, we measured neuropil fraction to represent the proportion of intercellular space occupied by synapses, dendrites, and axons.



Using this comparative frontal microstructural dataset, one aim was to determine which features are associated with variation in overall brain size. In addition, we predicted that species differences in microstructure across the primate phylogenetic tree would be more pronounced in prefrontal cortex compared to M1, as other neuroanatomical features of volumetric size and connectivity have evolved at varying rates (Goldman-Rakic 1988; Passingham and Wise 2012; Preuss and Goldman-Rakic 1991). Finally, we sought to test whether these microstructural features were associated with species-typical measures of cognitive function reported in the literature (i.e., self-control and domain-general cognitive test performance) (Deaner et al. 2007; MacLean et al. 2014).

# **Materials and methods**

### Tissue preparation

The sample was comprised of brains from 44 individuals, representing 14 different primate species (Fig. 1). Brains were collected opportunistically from subjects following death unrelated to the current study. All brains were from adults above the age of species-typical sexual maturity (Tacutu et al. 2018). Nonhuman primate specimens came from individuals that lived in zoos and research centers, and were maintained in accordance with each institution's animal care and use guidelines. Human brain samples were provided by the El Paso County coroner's office in Colorado from individuals with no reported history of neurological or psychiatric disorders. Left hemispheres were used when



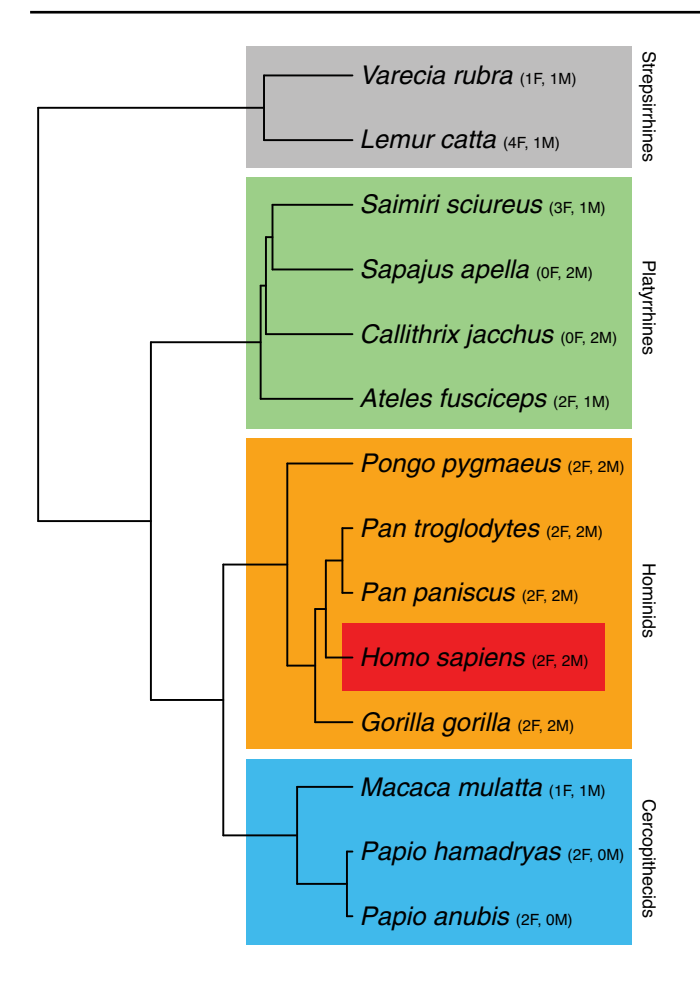


Fig. 1 Phylogenetic tree of the species included in this study, with sample sizes shown in parentheses

available (42 of 46 individuals). Within 24 h of each subject's death, the brain was removed and immersed in 10% formalin. In most cases, the brain was transferred to 0.1 M phosphate buffered saline (PBS) with 0.1% sodium azide solution after 10–14 days and stored at 4 °C. Whole hemispheres or blocks containing DLPFC, OFC, and M1 were cryoprotected by immersion in buffered sucrose solutions up to 30%, embedded in TBS freezing medium, frozen in a slurry of dry ice and isopentane, and sectioned at 40  $\mu$ m with a sliding microtome in the coronal plane.

### Regions of interest

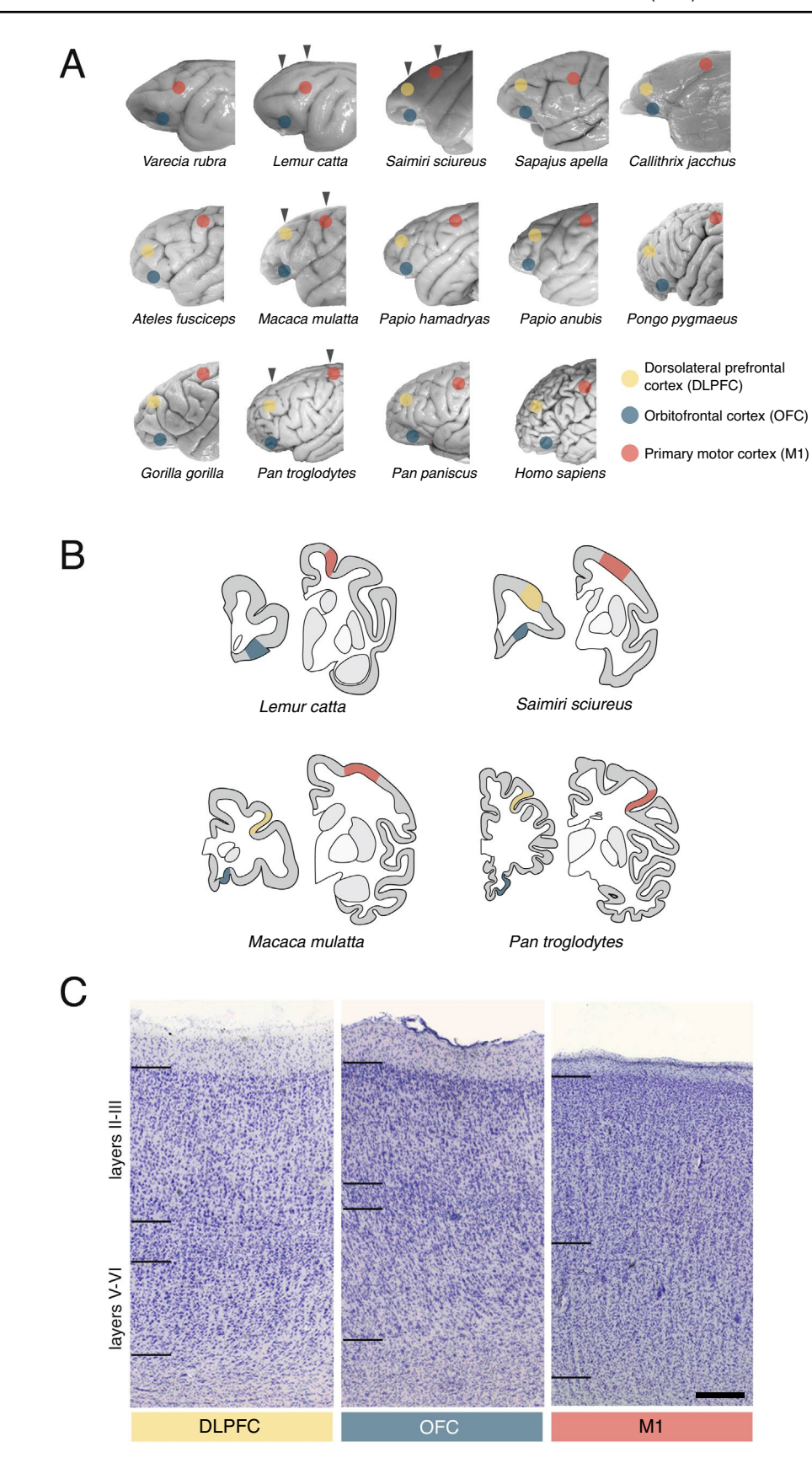
The two prefrontal regions included in our analyses, dorsolateral prefrontal cortex (DLPFC, area 46) and orbitofrontal cortex (OFC, area 13b), can be identified in the same coronal histological section in catarrhine primates (i.e., cercopithecid monkeys and apes). In platyrrhine monkeys, however, DLPFC is found slightly anterior to OFC (Fig. 2). There is no area 46 homologue identified in strepsirrhines, meaning this cortical subdivision likely evolved after haplorrhines diverged (Passingham and Wise 2012; Preuss and Goldman-Rakic 1991). Therefore, we included only OFC and M1 as regions of interest for the strepsirrhine species in the current study. The DLPFC is located laterally on the middle frontal gyrus above the inferior frontal gyrus in hominids; in cercopithecid monkeys, it is found within the principal sulcus. It is found on the coronal level just before the appearance of the corpus callosum in platyrrhines and just after it in cercopithecids, where the putamen becomes visible. The OFC is located on the ventral surface of the brain, along the medial orbital gyrus (Carmichael and Price 1994; Mai et al. 2007; Paxinos et al. 2008, 2011). Cytoarchitecturally, the DLPFC is granular, with larger neurons at the bottom of layer III and top of layer V. Layer IV is narrow and densely packed with small cells. The OFC is dysgranular and merges into agranular areas posteriorly (Carmichael and Price 1994; Hof et al 1995a; Preuss and Goldman-Rakic 1991; Semendeferi et al. 1998). Regions were traced along the superior frontal sulcus/principal sulcus (DLPFC) and medial orbital sulcus (OFC). The primary motor cortex (M1) is located on the anterior bank of the central sulcus. Cytoarchitecturally, M1 is identified by the presence of large Betz cells in layer V and the absence of a clear layer IV (Sherwood et al. 2003).

# **Neuropil fraction**

In each specimen, a 1:10 series of sections through each region was stained with 0.5% cresyl violet to reveal cytoarchitecture. Images of these Nissl-stained sections were acquired to quantify neuropil fraction (NF). Neuropil is the space within the grey matter, between the somata of neurons and glia, which remains unstained in Nissl-stained preparations, containing axons, dendrites, synapses, glial processes, and microvasculature (Issa et al. 2019; Spocter et al. 2012). We measured NF within each cortical area subdivided into supragranular layers II–III and infragranular layers V–VI. Supragranular and infragranular layers in the frontal cortex have been found to have differences in both cell morphology and axon density, which could indicate differences in neuropil space, projection length, or other functional differences (de Lima et al. 1990; Hof et al. 1995b; Raghanti et al. 2008a, b, 2009; Semendeferi et al. 1998). A systematic-random series of images was taken through each region of interest across three sections using a 20 x objective lens (average number of images = 95 for DLPFC; 93 for OFC; 102 for M1) with an Optronics MicroFire color video camera (Optronics, Golenta, CA), and a Zeiss Axioplan 2 photomicroscope (Zeiss, Thornwood, NY) equipped with a Ludl XY motorized stage (Ludl Electronics, Hawthorne, NY), Heidenhain z-axis encoder, coupled to a Dell PC workstation running StereoInvestigator software (MBF Bioscience, Williston, VT). The resulting images were 0.53 pixels/µm resolution. Each image was imported into Image J (v. 1.8.0 112; NIH,



Fig. 2 Cortical regions analyzed in this study. A Lateral views of frontal lobes, showing the cortical areas where data were collected. Images not to scale. Arrowheads indicate the coronal levels shown in panel B. B The location in coronal sections where regions were sampled for quantification, shown in representative species. C Histological appearance of cortical regions from Nissl staining in a chimpanzee brain. Scale bar = 250 μm





Bethesda, MD) and subjected to background subtraction with a rolling ball radius of 50 pixels and then converted to binary by an automated threshold routine (Spocter et al. 2012). Before calculation of the neuropil fraction, images that contained artifacts related to histological processing were removed from the batch. NF was calculated as the average across all images per individual per region and calculated as the space occupied by neuropil (white pixels) divided by the total number of pixels (Fig. 3).

# **Immunohistochemistry**

For immunohistochemical staining, four adjacent 1:10 series of free-floating sections from DLPFC, OFC and M1 were stained with: mouse monoclonal IgG<sub>1</sub> antibody against PV (1:10,000 dilution, 235, Swant, Switzerland; RRID:AB\_10000343); mouse monoclonal IgG<sub>1</sub> antibody against SERT (1:100,000 dilution, MAB5618, EMD Millipore, Billerica, MA; RRID:AB\_2190560); mouse monoclonal IgG<sub>1</sub> antibody against NEFH (1:3,000 dilution, 801,701, Biolegend, San Diego, CA; RRID:AB\_2564642); goat monoclonal IgG<sub>1</sub> antibody against TH (1:1,000 dilution, AB152, Millipore, Billerica, MA; RRID:AB\_390204) (Fig. 4).

Tyrosine hydroxylase (TH) is the rate-limiting enzyme in catecholamine synthesis, including dopamine (DA), epinephrine, and norepinephrine (Daubner et al. 2011). Studies in primates have shown that TH and DA-hydroxylase, the enzyme required for norepinephrine synthesis, are not extensively colocalized in axons within the cerebral cortex (Akil and Lewis 1993; Gaspar et al. 1989). Therefore, we interpret TH-positive axons in the current study to primarily represent dopaminergic innervation from the ventral tegmental area to the frontal cortex. However, it is important to note that norepinephrine-containing axons from the locus coeruleus may also play a significant role in cognitive processes

through effects on mood, motivation, attention, and arousal (Sara and Bouret 2012; Sharma et al. 2010).

Prior to immunostaining, sections were rinsed thoroughly in PBS and pretreated for antigen retrieval by incubation in 10 mM sodium citrate buffer (PV, TH: pH 3.5 at 37 °C in an oven; SERT, NEFH: pH 8.5 at 85 °C in a water bath) for 30 min then cooled at room temperature for an additional 20 min. Sections were then rinsed and immersed in a solution of 2.5% hydrogen peroxide in 75% methanol to eliminate endogenous peroxidase activity. After rinsing again, sections were incubated in solution containing PBS with normal horse serum and 0.1% Triton X-100 detergent for one hour and then incubated in primary antibody diluted in PBS for approximately 24 h on a rotator at 4 °C. After rinsing in PBS, sections were incubated in either biotinylated anti-mouse IgG (1:200 dilution, BA-2000, Vector Laboratories, Burlingame, CA) or biotinylated anti-goat (1:200 dilution, BA-1000, Vector Laboratories, Burlingame, CA) and processed with the avidin-biotin-peroxidase method using a Vectastain Elite ABC kit (pk-6100, Vector Laboratories). Sections were rinsed again in PBS, followed by a rinse in sodium acetate buffer. Immunoreactivity was revealed using 3,3'-diaminobenzidine and nickel enhancement according to a modification of the methods in Shu et al. (1988) as described in Van der Gucht et al. (2001). When the primary antibody was excluded in control experiments, no immunostaining was observed.

### Stereologic quantification

Three sections from the 1:10 series were quantified for each cortical region and marker using the same microscope setup as for NF measurement. In StereoInvestigator, contours were drawn around layers II–III and layers V–VI of each of the regions in every section under 4×magnification. Stereologic

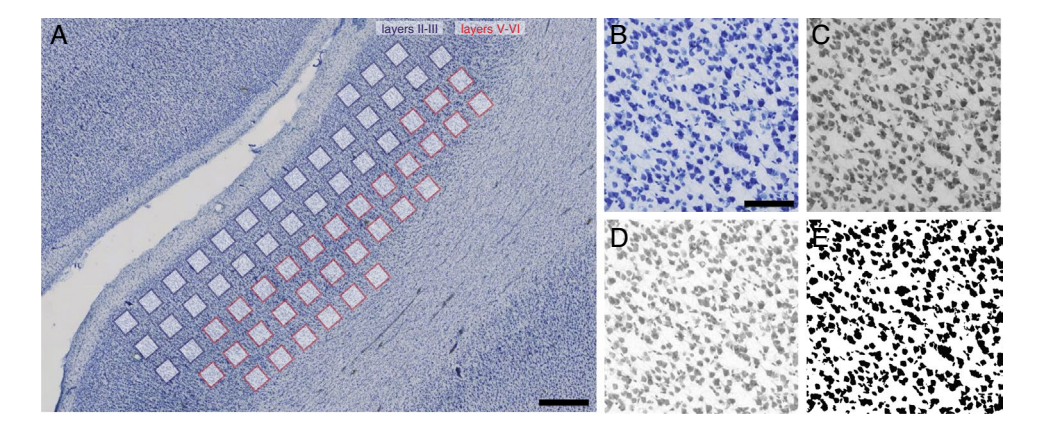


**Fig. 3** The procedure for obtaining neuropil fraction data. **A** A series of systematic random sampling of image frames is collected. The dorsolateral prefrontal cortex of a gorilla is shown as an example. Scale bar=500 µm. **B** Example of an image frame. Scale bar=150 µm. **C** 

Conversion to 8-bit greyscale. **D** Background subtraction using a rolling ball algorithm. **E** Binarization of the threshold image. The neuropil fraction is calculated as the proportion of the total pixels in the image that are white, representing the space surrounding cell bodies



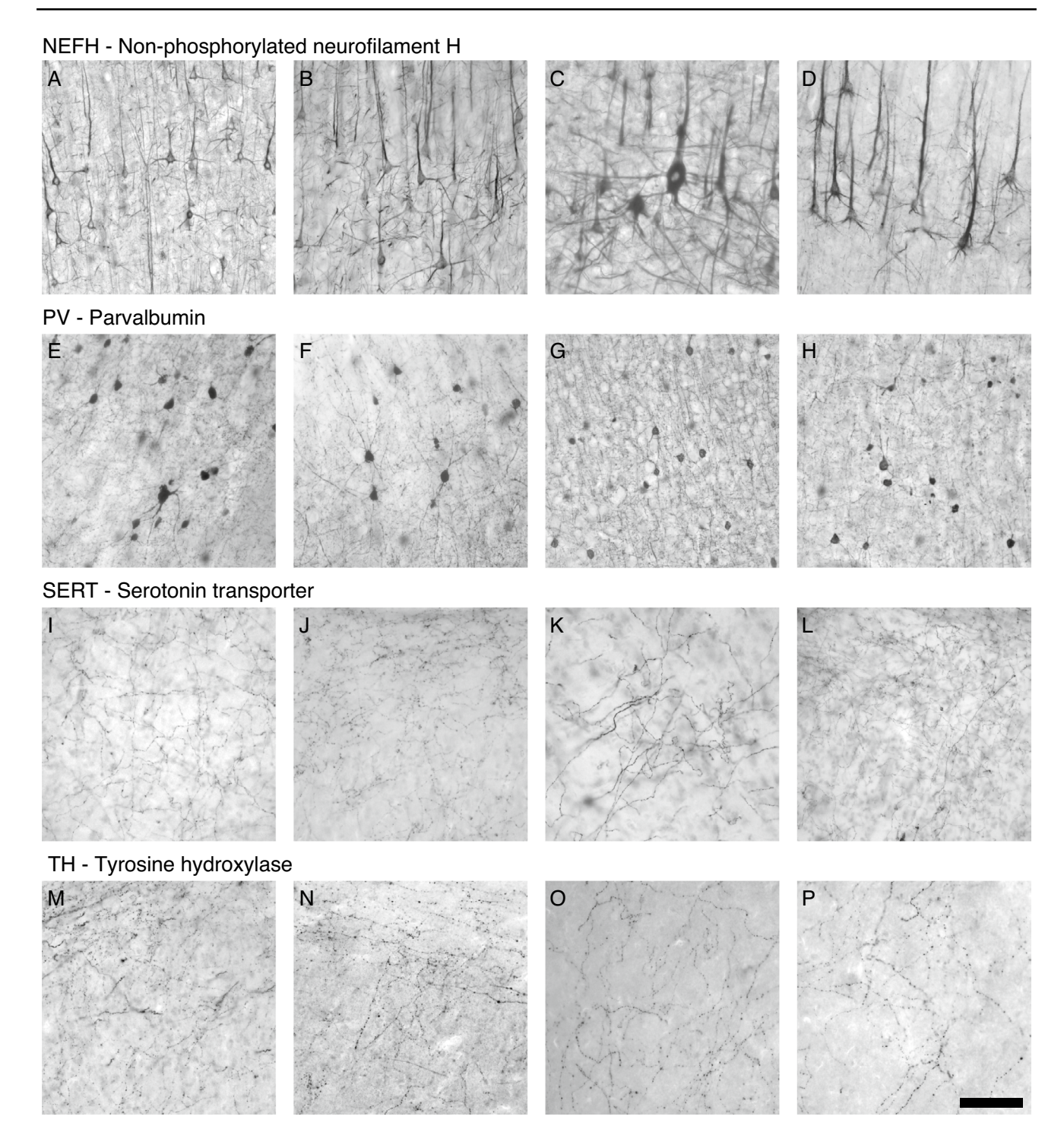


Fig. 4 Photomicrographs showing the immunostaining features that were quantified in this study. Non-phosphorylated neurofilament H in (A) DLPFC layer III of *Lemur catta*, B DLPFC layer III of *Ateles fusciceps*, C M1 layer V of *Sapajus apella*, D DLPFC layer III of *Pongo pygmaeus*. Parvalbumin in (E) DLPFC layer V of *Varecia rubra*, F DLPFC layer V of *Macaca mulatta*, G OFC layer V of *Callithrix jacchus*, H OFC layer V of *Saimiri sciureus*. Serotonin trans-

porter in (I) DLPFC layer III of Sapajus apella, (J) DLPFC layer III of Papio anubis, K DLPFC layer V of Gorilla gorilla, L M1 layer III of Pan troglodytes. Tyrosine hydroxylase in (M) OFC layer II of Macaca mulatta, N DLPFC layer II of Pongo pygmaeus, O DLPFC layer V of Homo sapiens, P DLPFC layer V of Homo sapiens. Scale bar = 100 µm



sampling was performed to measure the density of PV-immunoreactive (-ir) and NEFH-ir neurons, and length density of SERT-ir and TH-ir axons. Optical fractionator and Spaceballs analysis were performed to obtained estimates of neuron density and axon length density, respectively. Counts were collected under Koehler illumination using a 63×objective lens (Zeiss Plan-Apochromat, N.A. 1.4).

For neuron density, the counting frame was set at 65 μm × 65 μm. Neurons were counted using a counting frame height of 6 µm, with a guard zone of 1 µm at the top of the section. Cells were counted when the nucleus was located within the counting frame or on the green inclusion line. For axon length density, the radius of the hemisphere probe was set at 10 µm, with a 1 µm guard zone at the top of the section. Tissue was sampled in a systematic random fashion with the grid spacing optimized according to the specimen's region size. The sampling design was implemented with the goal of obtaining approximately 100 sampling sites per individual per region of interest. This yielded an average of  $132 \pm 35$  (standard deviation) sampling sites for PV-ir neurons,  $124 \pm 35$  sampling sites for NEFH-ir neurons,  $104 \pm 26$  sampling sites for SERT-ir axons, and  $107 \pm 21$  sampling sites for TH-ir axons. Total neuron density was calculated as the sum of neurons counted divided by the product of the sum of disectors examined and their volume (Sherwood et al. 2007).

Cellular volumes of NEFH-ir neurons were estimated using the nucleator probe with a vertical design (Gundersen 1988). Neurons were selected for volume measurement in a systematic random fashion by applying optical disector sampling in one section, as described above. The centroids of neurons included in optical disectors were marked and two transect lines from randomly selected directions were centered at the marker and superimposed over the neuron. The intersection of each line with the outer surface of the neuronal soma was marked and cellular volume was measured based on the nucleator principle. This sampling scheme resulted in the measurement of cellular volumes in an average of  $11 \pm 5$  NEFH-ir neurons for each region of interest per individual.

Total axon density was calculated as the total axon length over the planimetric reference volume as obtained from the StereoInvestigator software (Raghanti et al. 2008a). All numerical densities of both neurons and axons derived from these counts were corrected by the number-weighted mean section thickness as described in Sherwood et al. (2007).

# Quantifying trait changes and differences in rate of evolution

To provide an overview of the evolutionary changes that underpin the comparative variation in our data, we used Brownian motion (BM) to model the rate of phenotypic evolution (Adams 2014). Within BM, the evolution of a continuous trait "X" along a branch over time increment "t" is quantified as  $dX(t) = \sigma dB(t)$ , were " $\sigma$ " constitutes the magnitude of undirected, stochastic evolution and "dB(t)" is Gaussian white noise. BM-based modeling approaches model the accumulation of variance over time through its rate parameter " $\sigma^2$ ". The BM rate parameter has become the standard measure of evolutionary rate in phylogenetic comparative methods. We tested for differences in the BM rate parameter among measurements (NF, PV, NEFH, SERT, TH). Here, and for all subsequent analyses, we used the primate phylogeny provided by Arnold et al. (2010).

We performed a multi-regime Ornstein–Uhlenbeck (OU) modeling analysis (Khabbazian et al. 2016) on each microstructural variable relative to brain size. This analysis identifies the phylogenetic location of shifts in mean phenotypic value along particular branches in the phylogeny by quantifying the evolution of a continuous trait "X" as  $dX(t) = \alpha[\theta - X(t)]dt + \sigma dB(t)$  (Butler and King 2004). In this model, "\sigma" captures the stochastic evolution of a Brownian motion process, "\alpha" determines the rate of the adaptive evolution towards an optimum trait value "\theta". This standard OU model has been modified to accommodate for the possibility that traits may reach different optima across the phylogeny. Such multi-regime OU models allow modelling trait evolution towards different "regimes" that each display a different mean trait value.

### Correlations with brain size and cognition

To address whether these microstructural features are correlated with brain size, we regressed each variable against brain weight using phylogenetic least-squares analysis (Rohlf 2001) in combination with a maximum likelihood optimization of the degree of phylogenetic independence of the data using the lambda parameter (Pagel 1999). Least-squares model fitting further allowed identifying which variables indicate the best statistical fit with brain size by means of the Akaike information criterion (AIC).

To explore possible correlations with behavioral measures of cognition, we regressed each variable against two independent measures of cognition from the literature—self-control (MacLean et al. 2014) and domain-general cognitive test performance (Deaner et al. 2007). To measure self-control, MacLean et al. (2014) used two tests. The first method, known as the A-not-B task, involved subjects resisting the urge to search for food in a previously rewarded location when the food was visibly moved to a new location. The second method, called the cylinder task, required subjects to inhibit the impulse to directly reach for food hidden inside a transparent cylinder and instead use a detour response learned during familiarization. The percentage of test trials in which subjects performed the correct response



in each task was measured. These two tasks assessed different aspects of self-control, and a composite score was used to provide a broader measure across both tasks. Some have argued that because these tasks only measure the capacity to inhibit actions, they should be considered to represent only a partial measure of self-control (Beran 2018). The domain-general cognition variable used in this study was derived from a meta-analysis by Deaner et al. (2007). The meta-analysis combined results from various studies that investigated learning and cognition in multiple primate species, categorizing them into paradigms. The final dataset included information from 44 publications, comprising nine cognitive paradigms and 30 procedures. The species represented in the frontal cortex microstructure dataset overlapped with the self-control dataset except for Ateles fusciceps, Macaca mulatta, and Homo sapiens, and overlapped with the domain-general cognition dataset except for Pan paniscus and Homo sapiens. Because some microstructure variables were significantly correlated with brain size, we repeated the correlation analysis with cognitive measures by adding brain size as a predictor to models.

All hypothesis testing was two-tailed. We controlled for multiple testing using the procedure introduced by Benjamini and Hochberg (1995) and report the results based on both the unadjusted and adjusted alpha (*P* and *P*adj values).

# Results

Species averages for neuropil fraction, neuron densities, and axon densities can be found in Table 1. *Lemur catta* and *Varecia rubra* were not included in analyses of DLPFC, as a there is no homologous region to area 46 in strepsirrhines (Passingham and Wise 2012; Preuss and Goldman-Rakic 1991).

# Rates of evolution and phylogenetic regimes

Among the microstructure measurements (across regions and layers), neuropil fraction consistently showed a lower rate of evolution compared to other variables (P < 0.001). This result holds when separately considering different regions and/or layers and when considering variables scaled against brain size.

We used analysis of best-fit regime configurations to identify sets of lineages that display similar trait values for each microstructural variable relative to brain size. Only one variable was found to be divided into significantly different regimes between lineages in this dataset. Relative PV-ir neuron density (residuals after scaling to brain size) was lower in strepsirrhines compared to haplorrhines (AIC = 0.97). For every other microstructural variable, the best-fit OU model to the data indicated that a common slope and intercept

accounts for variation across phylogenetic groups of primates. Additionally, humans did not display significant differences in any of these microstructural variables compared to what would be predicted for their brain size.

### Correlations with brain size

Among measurements, neuropil fraction displayed the highest statistical fit with brain size (AIC $\Delta$  > 20). After adjusting results for multiple testing, 7 out of 36 (19%) of the microstructure measures were significantly associated with brain size, 5 of which were in OFC, 2 of which were in DLPFC, and none of which were in M1 (Table 2; Fig. 5). Neuropil fraction increases with brain size in OFC layers V-VI  $(b=0.030, P=0.008, P_{adj}=0.043)$ . NEFH-ir soma volume increases with brain size in DLPFC layers V–VI (b = 0.138, P = 0.006,  $P_{adi} = 0.035$ ). SERT-ir axon density decreases with brain size in OFC layers II–III (b = -0.239, P = 0.004,  $P_{adi} = 0.034$ ), OFC layers V-VI (b = -0.321, P = 0.001,  $P_{adi} = 0.015$ ), and DLPFC layers II-III (b = -0.255, P = 0.005,  $P_{adi} = 0.034$ ). TH-ir axon density decreases with brain size in OFC layers II-III (b = -0.433, P = 0.001,  $P_{adi} = 0.018$ ) and OFC layers V-VI (b = -0.457, P = 0.001,  $P_{adi} = 0.015$ ).

## **Correlations with cognition**

We examined the frontal cortex microstructural measures for correlations with published species-mean data on selfcontrol and domain-general cognitive test performance. After adjusting for multiple testing, only one microstructural variable displayed a correlation with data from the cognitive tests (Fig. 6). Neuropil fraction in OFC layers V-VI was positively correlated with self-control (b = 4.64, t = 6.57, P < 0.001,  $P_{adi} < 0.02$ ). This relationship remained significant when adding brain size as a covariate (neuropil fraction in OFC layer V–VI: b = 3.01, t = 6.42, P < 0.001; brain size: b=0.14, t=4.46, P<0.005). This analysis also indicates that neuropil fraction in OFC layers V-VI is a better predictor of self-control than brain size. Two additional analyses provided further confirmation of this result. Self-control predicted by neuropil fraction in OFC layers V-VI yielded an AIC value of -5.860, whereas self-control predicted by brain size yielded a lower AIC value of -3.485 (AIC $\Delta = 2.375$ ; AICw = 0.766). Lastly, a test of allometric integration (which compares rates of evolution of residual error; a lower rate indicating a higher integration, lower residual error and a better fit) revealed that predicting self-control by neuropil fraction in OFC layers V-VI yields a significantly lower rate of evolution than predicting self-control by brain size  $\sigma^2_{SC\sim NFOFCV-VI} = 0.0006985$ ,  $\sigma^2_{SC\sim Brainsize} = 0.003362$ , rate ratio: 4.813, P of difference in rates = 0.0155).



 Table 1
 Frontal cortex microstructure dataset from 14 primate species

Sample   S	Species	Mean brain wt		Sample size	Lay- ers	Neurop	Neuropil fraction		NEFH-ir mm3)	NEFH-ir neuron density (per mm3)	nsity (per	NEFH-ir (µm3)	NEFH-ir neuron volume (µm3)	lume	PV-ir net mm3)	PV-ir neuron density (per nm3)	ty (per	SERT-ir µm3)	SERT-ir axon density (µm/ µm3)	ity (µm/	TH-ir ax	TH-ir axon density (µm/µm3)	(µm/µm3)
1455.0         39.8         2F, 2 M         II-III         0.70         0.049         0.74           345.2         35.8         2F, 2 M         II-III         0.66         0.69         0.74           345.2         35.8         2F, 2 M         II-III         0.66         0.69         0.74           5.33.4         34.0         2F, 2 M         II-III         0.69         0.68         0.65           523.2         40.0         2F, 2 M         II-III         0.69         0.68         0.72           102.7         36.9         2F, 2 M         II-III         0.69         0.68         0.72           102.7         25.3         1F, 1 M         II-III         0.66         0.69         0.73           115.2         10.4         2F, 0 M         II-III         0.65         0.67         0.71           115.2         30.7         2F, 1 M         II-III         0.69         0.72         0.68           115.2         30.7         2F, 1 M         II-III         0.69         0.72         0.68           115.2         30.7         2F, 1 M         II-III         0.69         0.72         0.74           22.9         27.0         11-III<		(g)	sample (y)			DLPFC		M1	DLPFC	OFC	M1	DLPFC	OFC	M1	DLPFC	OFC	M1	DLPFC	OFC	M1	DLPFC	OFC	M1
345.2         35.8         2F.2 M         II-III         0.66         0.65         0.74           - 323.4         34.0         2F.2 M         II-III         0.66         0.65         0.65           523.2         34.0         2F.2 M         II-III         0.68         0.68         0.69           523.2         40.0         2F.2 M         II-III         0.66         0.68         0.69           102.7         25.3         1F.1 M         II-III         0.66         0.68         0.72           102.7         23.3         1F.1 M         II-III         0.66         0.69         0.72           115.9         10.4         2F.2 M         II-III         0.66         0.69         0.72           115.1         10.4         2F.2 M         II-III         0.65         0.67         0.73           115.2         30.7         2F.0 M         II-III         0.62         0.72         0.74           86.2         5.7         0F.2 M         II-III         0.69         0.65         0.74           8.0         5.7         0F.2 M         II-III         0.69         0.65         0.74           8.0         5.0         0F.2 M         II	Ното	1455.0	39.8	2F, 2 M	l	0.70	0.71	0.73	5740.1	6492.7	6880.1	2889.1	1810.3	1367.7	5123.6	5433.6	4490.9	0.0007	0.0009	0.0007	0.0003	0.0002	0.0005
345.2         35.8         2F, 2 M         II-III         0.66         0.65         0.65           - 323.4         34.0         2F, 2 M         II-III         0.69         0.66         0.69           523.2         40.0         2F, 2 M         II-III         0.69         0.68         0.72           523.2         40.0         2F, 2 M         II-III         0.69         0.68         0.72           102.7         25.3         1F, 1 M         II-III         0.69         0.68         0.72           102.7         23.3         1F, 1 M         II-III         0.66         0.69         0.72           151.9         10.4         2F, 2 M         II-III         0.66         0.69         0.73           151.9         10.4         2F, 0 M         II-III         0.60         0.69         0.73           151.9         10.4         2F, 0 M         II-III         0.62         0.63         0.71           151.9         10.4         2F, 0 M         II-III         0.69         0.65         0.71           152.0         2.7         1.4         1.4         1.4         0.62         0.62         0.72           152.1         2.5	sapiens				V-VI	0.70	0.69	0.74	4296.5	6478.6	5334.0	1830.2	1190.1	1159.6	2148.7	2459.2	1968.9	0.0006	0.0004	0.0004	0.0003	0.0003	0.0004
s-         323.4         34.0         2F,2 M         II-III         0.69         0.66         0.69           s-         323.4         34.0         2F,2 M         II-III         0.68         0.68         0.68         0.65           523.2         40.0         2F,2 M         II-III         0.66         0.68         0.72           335.0         36.9         2F,2 M         II-III         0.66         0.68         0.73           1         102.7         23.3         IF,1 M         II-III         0.66         0.69         0.73           2         151.9         10.4         2F,0 M         II-III         0.66         0.69         0.73           3         151.9         10.4         2F,0 M         II-III         0.60         0.69         0.73           4         151.2         30.7         2F,1 M         II-III         0.60         0.62         0.73           5         115.2         30.7         2F,1 M         II-III         0.69         0.65         0.74           6         115.2         30.7         2F,1 M         II-III         0.69         0.65         0.74           8         2         2         2	Pan trog-	345.2	35.8	2F, 2 M		99.0	0.65	0.65	4748.9	3636.0	12,360.2	1377.0	1454.1	1644.0	3851.2	3224.4	4144.7	0.0018	0.0029	0.0035	0.0009	0.0007	0.0021
5-         323.4         34.0         2F, 2 M         II-III         0.68         0.68         0.72           523.2         40.0         2F, 2 M         II-III         0.66         0.68         0.72           335.0         36.9         2F, 2 M         II-III         0.66         0.68         0.73           102.7         23.3         1F, 1 M         II-III         0.66         0.69         0.67           151.9         10.4         2F, 0 M         II-III         0.66         0.69         0.67           8-         151.9         10.4         2F, 0 M         II-III         0.66         0.69         0.73           8-         151.9         10.4         2F, 0 M         II-III         0.60         0.68         0.73           8-         115.2         30.7         2F, 1 M         II-III         0.60         0.62         0.70           8-         115.2         30.7         2F, 1 M         II-III         0.69         0.65         0.74           8-         115.2         30.7         2F, 1 M         II-III         0.69         0.65         0.74           8-         115.2         37         0F, 2 M         II-III         0	lodytes				V-VI		99.0	69.0	5395.6	4229.7	6992.6	1092.6	1028.9	1437.6	3057.4	2193.8	2101.3	0.0015	0.0020	0.0027	0.0010	0.0008	0.0012
10   10   10   10   10   10   10   10	Pan panis-	323.4	34.0	2F, 2 M		89.0	0.68	0.65	2396.8	3278.5	7618.8	1311.8	1348.3	1773.7	5448.2	4541.7	5232.2	0.0019	0.0025	0.0028	0.0008	0.0008	600000
523.2         40.0         2F, 2 M         II-III         0.66         0.68         0.72           335.0         36.9         2F, 2 M         II-III         0.66         0.64         0.67           102.7         23.3         IF, 1 M         II-III         0.66         0.69         0.67           151.9         10.4         2F, 0 M         II-III         0.66         0.69         0.67           138.2         6.3         2F, 0 M         II-III         0.62         0.68         0.73           5-         115.2         30.7         2F, 0 M         II-III         0.69         0.67         0.68           86.2         2F, 0 M         II-III         0.64         0.65         0.73         0.74           86.2         30.7         2F, 1 M         II-III         0.69         0.72         0.68           86.2         5.7         0F, 2 M         II-III         0.69         0.75         0.68           8         2.5         0F, 2 M         II-III         0.69         0.65         0.74           8         2.0         0F, 2 M         II-III         0.69         0.65         0.68           8         2.0         0F, 2 M </td <td>cus</td> <td></td> <td></td> <td></td> <td>V-VI</td> <td></td> <td>0.68</td> <td>0.72</td> <td>2208.7</td> <td>2134.0</td> <td>4570.9</td> <td>1202.1</td> <td>922.7</td> <td>1269.2</td> <td>4168.2</td> <td>3803.2</td> <td>4635.2</td> <td>0.0017</td> <td>0.0015</td> <td>0.0018</td> <td>0.0005</td> <td>0.0006</td> <td>0.0005</td>	cus				V-VI		0.68	0.72	2208.7	2134.0	4570.9	1202.1	922.7	1269.2	4168.2	3803.2	4635.2	0.0017	0.0015	0.0018	0.0005	0.0006	0.0005
335.0   36.9   2F,2 M   II-III   0.66   0.64   0.07     102.7   23.3   1F,1 M   II-III   0.66   0.69   0.67   0.75     151.9   10.4   2F,0 M   II-III   0.65   0.68   0.73     151.9   10.4   2F,0 M   II-III   0.62   0.68   0.73     138.2   6.3   2F,0 M   II-III   0.64   0.65   0.70     5-   115.2   30.7   2F,1 M   II-III   0.69   0.72   0.68     86.2   5.7   0F,2 M   II-III   0.69   0.72   0.68     86.3   2.5   3F,1 M   II-III   0.69   0.75   0.68     8   8   8   8   8   8   8   8   8	Gorilla	523.2	40.0	2F, 2 M		99.0	0.68	0.72	5341.5	3691.2	4985.0	1534.1	1076.9	2278.1	3388.8	4002.9	2610.2	0.0014	0.0020	0.0018	0.0004	0.0004	0.0010
335.0   36.9   2F, 2 M   II-III   0.66   0.64   0.67     102.7   23.3   1F, 1 M   II-III   0.66   0.69   0.67     151.9   10.4   2F, 0 M   II-III   0.65   0.68   0.73     138.2   6.3   2F, 0 M   II-III   0.64   0.65   0.75     5-   115.2   30.7   2F, 1 M   II-III   0.69   0.72   0.68     86.2   5.7   0F, 2 M   II-III   0.69   0.72   0.68     86.3   2.5   3F, 1 M   II-III   0.69   0.72   0.68     86.4   2.5   3F, 1 M   II-III   0.65   0.65   0.74     87   22.9   23.5   3F, 1 M   II-III   0.65   0.65   0.65     88   80   5.0   0F, 2 M   II-III   0.65   0.65   0.65     89   23.5   20.5   4F, 1 M   II-III   0.44   0.65   0.65     80   23.5   4F, 1 M   II-III   0.45   0.65   0.65     80   23.5   4F, 1 M   II-III   0.45   0.65   0.65     80   23.5   4F, 1 M   II-III   0.45   0.65   0.65     80   23.5   4F, 1 M   II-III   0.45   0.65   0.65     80   23.5   20.5   4F, 1 M   II-III   0.45   0.65   0.65     80   23.5   20.5   4F, 1 M   II-III   0.45   0.65   0.65     80   23.5   20.5   4F, 1 M   II-III   0.45   0.65   0.65     80   23.5   20.5   4F, 1 M   II-III   0.45   0.65   0.65     80   23.5   20.5   4F, 1 M   II-III   0.45   0.65   0.65     80   23.5   20.5   4F, 1 M   II-III   0.45   0.65   0.65     80   23.5   20.5   4F, 1 M   II-III   0.45   0.65   0.65     80   23.5   20.5   20.5   20.5   20.5   0.65     80   20.5   20.5   20.5   20.5   20.5   20.5     80   20.5   20.5   20.5   20.5   20.5   20.5     80   20.5   20.5   20.5   20.5   20.5   20.5     80   20.5   20.5   20.5   20.5   20.5   20.5     80   20.5   20.5   20.5   20.5   20.5   20.5     80   20.5   20.5   20.5   20.5   20.5   20.5     80   20.5   20.5   20.5   20.5   20.5     80   20.5   20.5   20.5   20.5   20.5     80   20.5   20.5   20.5   20.5     80   20.5   20.5   20.5   20.5   20.5     80   20.5   20.5   20.5   20.5   20.5     80   20.5   20.5   20.5   20.5   20.5     80   20.5   20.5   20.5   20.5   20.5     80   20.5   20.5   20.5   20.5   20.5     80   20.5   20.5   20.5   20.5     80   20.5   20.5   20.5   20.5     80   20.5   20.5   20.5	gorilla				V-VI	69.0	89.0	0.78	4612.1	2995.5	3837.7	2073.5	1003.0	1026.5	2430.4	3059.9	2414.4	0.0008	0.0011	0.0010	0.0003	0.0003	0.0005
102.7   23.3   1F, 1M   1I-III   0.66   0.69   0.67   0.75     151.9   10.4   2F, 0M   1I-III   0.62   0.68   0.73     151.8   10.4   2F, 0M   1I-III   0.62   0.68   0.73     138.2   6.3   2F, 0M   1I-III   0.64   0.65   0.71     15.5   20.7   2F, 1M   1I-III   0.69   0.72   0.68     15.5   20.5   2F, 1M   1I-III   0.69   0.72   0.68     15.5   20.5   2F, 1M   1I-III   0.69   0.72   0.68     15.5   20.5   2F, 1M   1I-III   0.65   0.65   0.67     15.5   20.5   2F, 1M   2F,	Pongo	335.0	36.9	2F, 2 M		99.0	0.64	0.67	4423.6	2220.8	5033.8	1463.3	1558.2	2622.9	3042.4	3106.6	2359.1	0.0024	0.0035	0.0022	0.0006	0.0008	0.0003
102.7   23.3   1F, 1 M   11—III   0.66   0.69   0.67     151.9   10.4   2F, 0 M   11—III   0.62   0.68   0.73     138.2   6.3   2F, 0 M   11—III   0.64   0.65   0.75     2	pyg- maeus				V-VI		0.67	0.75	3116.9	2649.0	3192.2	1479.7	918.3	1584.8	2146.0	2453.9	3398.6	0.0020	0.0023	0.0023	0.0003	0.0004	0.0010
151.9   10.4   2F, 0M   II-III   0.62   0.68   0.73     151.9   10.4   2F, 0M   II-III   0.65   0.66   0.75     138.2   6.3   2F, 0M   II-III   0.64   0.65   0.71	Масаса	102.7	23.3	1F, 1 M			69.0	0.67	5666.7	5594.4	4811.0	1217.4	1088.9	2163.0	3473.7	2494.8	1995.0	0.0013	0.0021	0.0011	0.0015	0.0020	0.0019
151.9   10.4   2F, 0 M   II-III   0.62   0.68   0.73     138.2   6.3   2F, 0 M   II-III   0.64   0.65   0.75     138.2   6.3   2F, 0 M   II-III   0.64   0.65   0.71     2.5   115.2   30.7   2F, 1 M   II-III   0.69   0.72   0.68     86.2   5.7   0F, 2 M   II-III   0.64   0.68   0.74     86.2   5.7   0F, 2 M   II-III   0.64   0.68   0.74     7   22.9   23.5   3F, 1 M   II-III   0.65   0.65   0.65     8   8   8   5.0   0F, 2 M   II-III   0.65   0.65   0.67     8   8   8   5.0   0F, 2 M   II-III   0.65   0.65   0.67     9   7   7   7   0.72   0.64   0.76     9   7   7   0.72   0.64   0.76     9   7   7   0.72   0.64   0.76     9   7   7   0.72   0.64   0.76     9   7   7   0.72   0.64   0.76     9   7   0.72   0.64   0.76     9   7   0.72   0.64   0.76     9   7   0.72   0.64   0.76     9   7   0.72   0.64   0.76     9   7   0.72   0.64   0.76     9   7   0.72   0.64   0.76     9   7   0.72   0.64   0.76     9   7   0.72   0.64   0.76     9   7   0.72   0.64   0.76     9   7   0.72   0.64   0.76     9   7   0.72   0.64   0.76     9   7   0.72   0.64   0.76     9   7   0.72   0.64   0.76     9   7   0.72   0.64   0.76     9   7   0.72   0.64   0.76     9   0.72   0.72   0.64     9   0.72   0.72   0.72     9   0.72   0.7	mulatta				V-VI		89.0	0.73	5759.6	4068.8	7520.0	1215.7	1117.1	1174.3	2176.2	2049.6	1507.6	0.0010	0.0016	0.0014	0.0013	0.0020	0.0017
y-VI         0.65         0.66         0.75           138.2         6.3         2F, 0 M         II-III         0.64         0.65         0.71           y-VI         0.62         0.62         0.70         0.71         0.62         0.71           y-VI         0.63         0.72         0.62         0.72         0.68         0.74           86.2         5.7         0F, 2 M         II-III         0.69         0.72         0.68           86.2         5.7         0F, 2 M         II-III         0.63         0.74         0.74           86.2         5.7         0F, 2 M         II-III         0.63         0.65         0.74           86.2         5.7         0F, 2 M         II-III         0.65         0.65         0.65           8         8.0         5.0         0F, 2 M         II-III         0.64         0.66         0.67           8         8.0         5.0         0F, 2 M         II-III         N/A         0.62         0.69           8         8.0         1F, 1 M         II-III         N/A         0.62         0.67           9         2.0.5         4F, 1 M         II-III         N/A         0.62	Papio	151.9	10.4	2F, 0 M		0.62	89.0	0.73	4325.7	3135.1	5459.9	1244.8	1426.7	1693.2	5628.6	2607.4	2841.3	0.0029	0.0042	0.0017	0.0008	0.0009	0.0007
138.2 6.3 2F, 0 M II-III 0.64 0.65 0.71  y-V1 0.62 0.62 0.70  y-V1 0.62 0.62 0.70  y-V1 0.71 0.69 0.72 0.68  86.2 5.7 0F, 2 M II-III 0.64 0.68 0.74  y-V1 0.71 0.69 0.74  y-V1 0.62 0.65 0.74  y-V1 0.62 0.65 0.74  y-V1 0.62 0.65 0.74  y-V1 0.62 0.65 0.74  y-V1 0.65 0.65 0.68  y-V1 0.72 0.64 0.68  y-V1 0.72 0.64 0.67  y-V1 0.72 0.64 0.67  y-V1 0.72 0.64 0.76  y-V1 0.72 0.64 0.76  y-V1 0.72 0.64 0.76  y-V1 0.72 0.64 0.76  y-V1 0.71 0.72 0.64 0.76  y-V1 0.72 0.64 0.76  y-V1 0.71 0.72 0.64 0.76  y-V1 0.72 0.64 0.76  y-V1 0.73 0.65 0.67  y-V1 0.74 0.75 0.69  y-V1 0.75 0.67	anubis				V-VI		99.0	0.75	5920.2	3932.5	4182.7	1629.7	1681.1	2055.4	6837.5	3256.5	2193.9	0.0022	0.0026	0.0010	0.0009	0.0009	0.0004
8-2 115.2 30.7 2F, 1 M II-III 0.69 0.72 0.68 8-2 5.7 0F, 2 M II-III 0.69 0.72 0.68 8-2 5.7 0F, 2 M II-III 0.64 0.68 0.74 7-V1 0.62 0.65 0.74 8-2 2.9 23.5 3F, 1 M II-III 0.65 0.65 0.65 8-8 8-9 0F, 2 M II-III 0.65 0.66 0.67 8-8 8-9 0F, 2 M II-III 0.65 0.66 0.67 8-9 0F, 2 M III-III 0.65 0.64 0.76 8-9 0F, 2 M III-III 0.65 0.64 0.76 8-9 0F, 2 M III-III 0.75 0.64 0.76 8-9 0F, 2 M III-III 0.75 0.64 0.76 8-9 0F, 2 M III-III 0.75 0.65 0.67	Papio	138.2	6.3	2F, 0 M		0.64	0.65	0.71	5864.4	4792.8	6852.7	1880.9	1646.8	1578.6	3352.9	2463.7	3144.3	0.0019	0.0028	0.0013	0.0005	0.0008	0.0005
s-         115.2         30.7         2F, 1 M         II-III         0.69         0.72         0.68           86.2         5.7         0F, 2 M         II-III         0.64         0.69         0.74           22.9         23.5         3F, 1 M         II-III         0.63         0.65         0.74           x         8.0         23.5         3F, 1 M         II-III         0.65         0.65         0.67           x         8.0         5.0         0F, 2 M         II-III         0.65         0.67         0.67           x         8.0         5.0         0F, 2 M         II-III         0/A         0.62         0.59           x         23.5         20.5         4F, 1 M         II-III         N/A         0.62         0.67           x         23.5         20.5         1F, 1 M         II-III         N/A         0.62         0.67           30.8         22.6         1F, 1 M         II-III         N/A         0.58         0.61	hama- dryas				V-VI		0.62	0.70	6893.9	5471.0	3342.9	1118.0	2041.2	1870.2	4734.5	1388.9	1593.0	0.0016	0.0019	0.0010	0.0005	0.0010	0.0002
N-Min   N-Mi	Ateles fus-	115.2	30.7	2F, 1 M		69.0	0.72	89.0	8193.1	7040.1	6895.4	2026.7	1524.0	2073.8	5029.2	3946.0	2750.8	0.0025	0.0037	0.0015	0.0014	0.0024	0.0014
86.2   5.7   0F, 2 M   II-III   0.64   0.68   0.70     V-VI   0.62   0.65   0.74     V-XI   0.62   0.65   0.74     V-XI   0.63   0.65   0.74     V-XI   0.54   0.55   0.68     V-XI   0.55   0.66   0.67     V-XI   0.71   0.72   0.64   0.76     V-XI   0.72   0.64   0.76     V-XI   0.74   0.75   0.64     V-XI   0.74   0.75   0.69     V-XI   0.75   0.75     V-XI	ciceps				V-VI		69.0	0.74	8666.3	6294.9	4405.2	1442.7	1582.8	2463.7	3830.3	2546.9	2536.6	0.0015	0.0025	0.0008	0.0014	0.0020	0.0009
i     22.9     23.5     3F, 1 M     II-III     0.53     0.58     0.62     0.74     9       eeus     V-VI     0.56     0.55     0.68     0.62     0.75       rix     8.0     5.0     0F, 2 M     II-III     0.65     0.66     0.67       us     V-VI     0.72     0.64     0.76       23.5     20.5     4F, 1 M     II-III     N/A     0.62     0.59     1       v     V-VI     N/A     0.62     0.67     1       v     V-VI     II-III     N/A     0.62     0.67     1	Sapajus	86.2	5.7	0F, 2 M		0.64	0.68	0.70	7252.0	5017.2	13,337.4	1575.3	1197.4	1037.9	3887.5	2999.7	4743.4	0.0035	0.0050	0.0024	0.0020	0.0023	0.0031
i     22.9     23.5     3F, 1 M     II-III     0.53     0.58     0.62     3.62       veats     vevt     0.56     0.55     0.68     0.68     0.68       rix     8.0     5.0     0F, 2 M     II-III     0.65     0.66     0.67     3       uss     vevt     0.72     0.64     0.76     3       23.5     20.5     4F, 1 M     II-III     N/A     0.62     0.59     1       vevt     vevt     N/A     0.62     0.67     1       vevt     vevt     N/A     0.62     0.67     1       vevt     vevt     II-III     N/A     0.58     0.61     1	apella				V-VI		0.65	0.74	9236.7	7945.3	10,167.7	1168.6	1112.1	2143.0	3838.7	1761.8	2733.0	0.0020	0.0020	0.0019	0.0023	0.0024	0.0017
rix 8.0 5.0 0F, 2 M II-III 0.65 0.55 0.68 rix 8.0 5.0 0F, 2 M II-III 0.65 0.66 0.67 8 0.68 0.55 0.68 0.67 8 0.68 0.57 0.64 0.76 0.57 0.58 0.59 0.59 0.59 0.59 0.59 0.59 0.59 0.59	Saimiri	22.9	23.5	3F, 1 M		0.53	0.58	0.62	5390.2	3121.9	8701.7	1217.2	1432.1	1670.5	4861.8	3386.8	2471.9	0.0029	0.0046	0.0021	0.0011	0.0012	0.0022
nts 8.0 5.0 0F, 2 M II—III 0.65 0.66 0.67  nus 23.5 20.5 4F, 1 M II—III N/A 0.62 0.59  V—VI N/A 0.62 0.59  V—VI N/A 0.62 0.69	sciureus				V-VI		0.55	89.0	7914.8	7258.5	5843.9	1191.4	8.586	1233.3	4809.7	5568.7	1404.8	0.0023	0.0033	0.0016	0.0011	0.0014	0.0013
V-VI 0.72 0.64 0.76 7 23.5 20.5 4F, 1 M II-III N/A 0.62 0.59 1 V-VI N/A 0.62 0.67 1 a 30.8 22.6 IF, 1 M II-III N/A 0.58 0.61 1	Callithrix	8.0	5.0	0F, 2 M		0.65	99.0	0.67	8104.4	3544.5	8.299.8	938.3	1084.1	904.6	3419.9	3070.4	2901.1	0.0036	0.0056	0.0022	0.0009	0.0014	0.0011
23.5 20.5 4F, 1 M II-III N/A 0.62 0.59 V-VI N/A 0.62 0.67 a 30.8 22.6 1F, 1 M II-III N/A 0.58 0.61	jacchus				V-VI		0.64	0.76	7824.6	3269.2	9.8089	794.9	668.4	1029.1	5968.1	4708.7	8080.7	0.0023	0.0031	0.0024	0.0007	0.0015	0.0010
V-VI N/A 0.62 0.67 30.8 22.6 IF, I M II–III N/A 0.58 0.61	Lemur	23.5	20.5	4F, 1 M		N/A	0.62	0.59	N/A	5918.3	12,681.6	N/A	1327.1	1256.6	N/A	1413.5	3069.3	N/A	0.0026	0.0015	N/A	0.0034	0.0030
30.8 22.6 1F, 1 M II-III N/A 0.58 0.61	catta				V-VI		0.62	0.67	N/A	4941.6	11,743.8	N/A	1151.3	1058.8	N/A	1074.7	2110.5	N/A	0.0025	0.0011	N/A	0.0030	0.0018
	Varecia	30.8	22.6	1F, 1 M			0.58	0.61	N/A	7469.2	10,890.1	N/A	1755.6	1471.9	N/A	2051.9	2644.3	N/A	0.0041	0.0041	N/A	0.0032	0.0022
V-VI N/A 0.60 0.68	rubra				V-VI	N/A	09.0	99.0	N/A	5700.0	6738.7	N/A	1827.4	1664.7	N/A	1376.8	1869.2	N/A	0.0045	0.0017	N/A	0.0035	0.0009



**Table 2** Associations between brain size and microstructural variables

Microstructural variable	Region	Layers	P Value	Adjusted P Value	Slope (b)	AIC Value
Neuropil fraction	DLPFC	II–III	0.056	0.108	0.029	-26.9
		V–VI	0.367	0.441	0.015	-23.0
	OFC	II–III	0.038	0.102	0.026	-34.6
		V-VI	0.008	0.043	0.030	-38.6
	M1	II–III	0.032	0.096	0.033	-36.5
		V-VI	0.197	0.273	0.012	-40.7
NEFH-ir neuron density	DLPFC	II–III	0.147	0.211	-0.106	11.8
		V-VI	0.030	0.096	-0.193	14.8
	OFC	II–III	0.722	0.743	-0.027	18.2
		V-VI	0.444	0.500	-0.062	20.0
	M1	II–III	0.138	0.211	-0.105	15.2
		V-VI	0.086	0.141	-0.131	16.9
NEFH-ir neuron volume	DLPFC	II–III	0.015	0.061	0.143	4.1
		V-VI	0.006	0.035	0.138	-1.0
	OFC	II–III	0.323	0.401	0.035	-3.6
		V-VI	0.070	0.126	0.148	9.7
	M1	II–III	0.057	0.108	0.108	8.3
		V-VI	0.800	0.800	0.015	12.3
PV-ir neuron density	DLPFC	II–III	0.669	0.708	0.022	4.5
		V-VI	0.024	0.087	-0.188	13.0
	OFC	II–III	0.042	0.102	0.138	5.2
		V-VI	0.440	0.500	-0.090	24.4
	M1	II–III	0.205	0.274	0.073	9.9
		V-VI	0.551	0.601	-0.057	25.1
SERT-ir axon density	DLPFC	II–III	0.005	0.034	-0.255	13.0
		V-VI	0.013	0.060	-0.216	13.4
	OFC	II–III	0.004	0.034	-0.239	15.5
		V-VI	0.001	0.015	-0.321	17.9
	M1	II–III	0.276	0.355	-0.102	23.7
		V-VI	0.141	0.211	-0.150	25.5
TH-ir axon density	DLPFC	II–III	0.044	0.102	-0.236	21.9
-		V–VI	0.075	0.128	-0.259	27.7
	OFC	II–III	0.001	0.018	-0.433	28.4
		V–VI	0.001	0.015	-0.457	27.3
	M1	II–III	0.045	0.102	-0.277	32.9
		V-VI	0.056	0.108	-0.315	38.0

## **Discussion**

The present study investigated the evolutionary scaling and cognitive correlates of primate frontal cortex microstructure. Neuropil fraction showed a lower rate of evolution compared to other variables, and it displayed the highest statistical fit with brain size. Additionally, humans did not display significant differences in any of these microstructural variables compared to what would be predicted for their brain size, suggesting that scaling is a major determinant of the microstructure of the human frontal cortex. Neuropil fraction in OFC layers V–VI was positively correlated with self-control, and this relationship remained significant when adding brain

size as a covariate, indicating that neuropil fraction in OFC layers V–VI is a better predictor of self-control than brain size and, thus, may contribute to species differences in the regulation of behavior. This finding is particularly interesting given the well-established role of the OFC in reward processing and decision-making in humans and other primates (Rolls 2004). Notably, the integrity of the OFC was shown to contribute more than the DLPFC in marmosets to their performance on a detour reaching task similar to the comparative self-control measures in the dataset we used for our analyses (Wallis et al. 2001).

Neuropil is a fundamental component of the cerebral cortex that consists of the tissue surrounding the somata



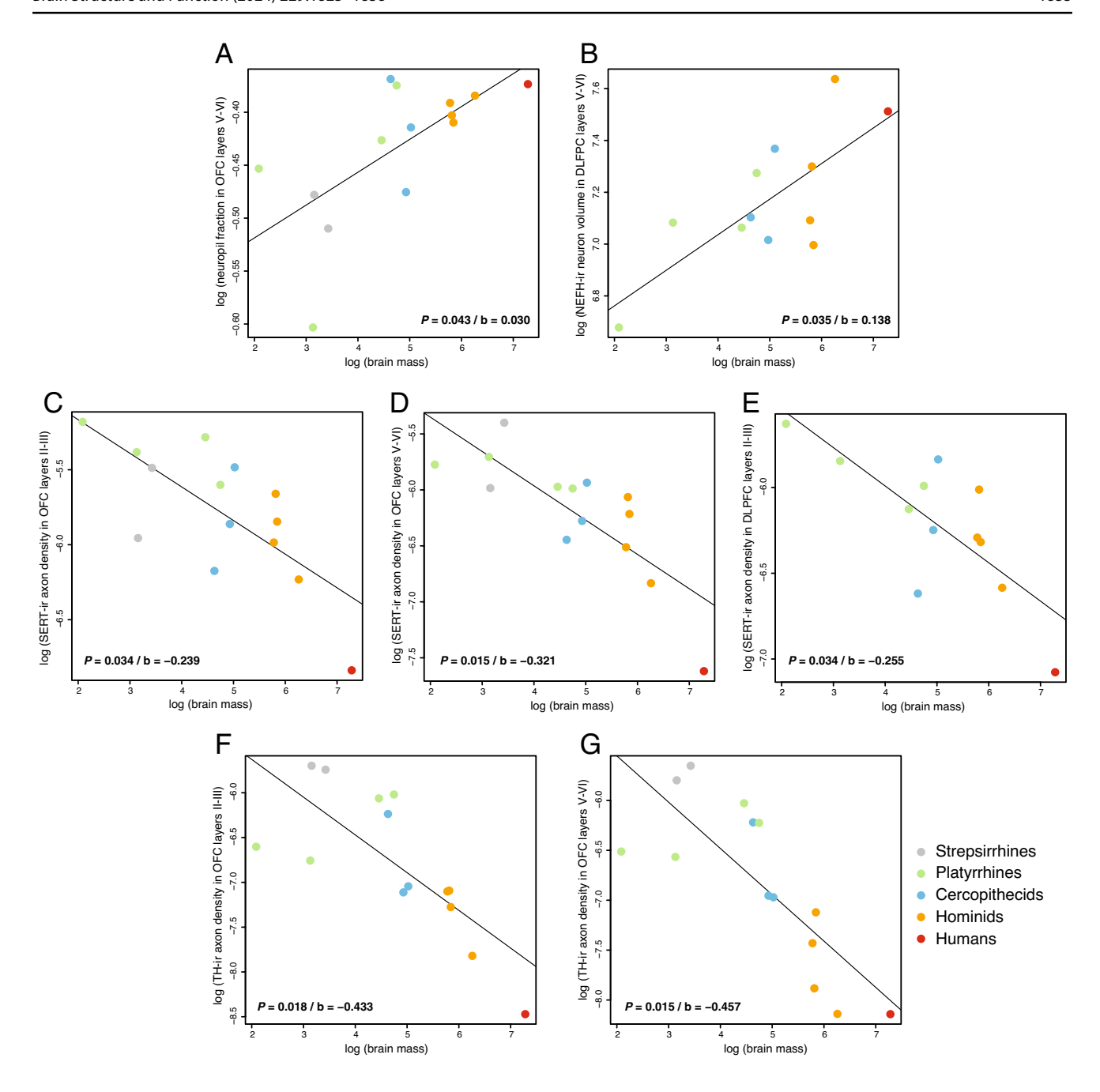


**Fig. 5** Bivariate plots of the microstructural variables that were significantly correlated with brain size after correcting for multiple comparisons. Adjusted *P* values are shown

of cells and includes elements such as axons, dendrites, and glial cell processes. The fact that neuropil fraction displays the strongest overall association with brain size in our analysis may reflect the need for more connections and synapses per neuron to support the maintenance of networks in larger brains (Rash et al. 2023; Semendeferi et al. 2011; Sherwood et al. 2020; Spocter et al. 2012). Species that have cortices with more neuropil space, such as humans, great apes, and elephants, also have networks of

larger, more complex neurons with greater dendritic arborization (Bianchi et al. 2013; Elston et al. 2011; Jacobs et al. 2001, 2011). In contrast, other microstructural variables, such as interneuron proportions, may serve functions in the cortex that are more constrained to be relatively invariant or less linked with brain size across primate lineages (Fishell and Kepecs 2020; Sherwood et al. 2007; Shi et al. 2021). Overall, the slower rate of evolution and strong association with brain size of neuropil suggest that



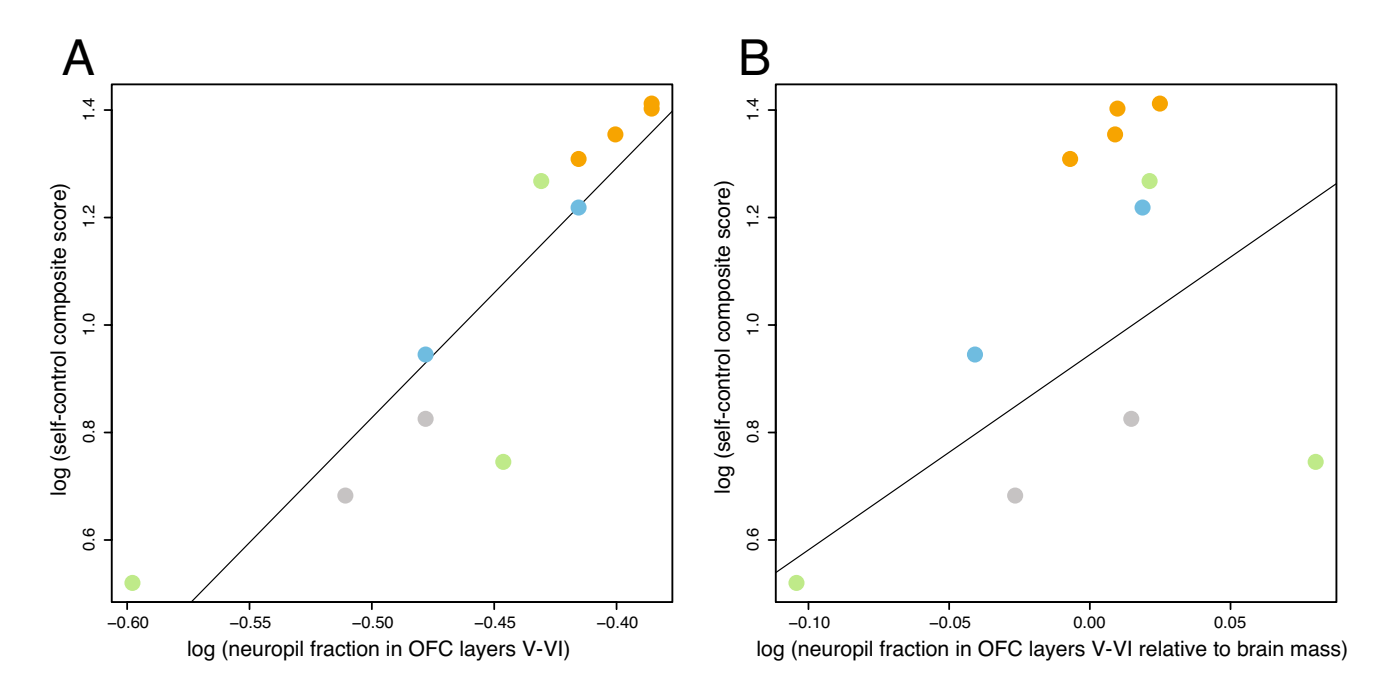


Fig. 6 Bivariate plots of the significant correlation between neuropil fraction in OFC layers V-VI and self-control composite score. Data-point color legend from Fig. 5

it plays a fundamental role that scales allometrically in the primate cerebral cortex.

Dopaminergic (i.e., TH-ir) and serotonergic (i.e., SERTir) axon length density were found to significantly decrease with brain size across the primate species examined. This occurs in conjunction with the well-known pattern of neuron density also decreasing in larger brains (Herculano-Houzel et al. 2007; Sherwood et al. 2020). Further research is needed to explore the underlying mechanisms and functional implications of these coordinated changes in axon and neuron densities across primate species. In previous comparative studies focusing on human, chimpanzee, and macaque brains, we calculated the ratio of dopaminergic and serotonergic axon length density relative to neuron density to estimate the amount of potential innervation per neuron (Raghanti et al. 2008a, b). We found that human and chimpanzee brains exhibited a higher relative innervation density compared to macaque monkeys in layers V-VI of prefrontal areas 9 and 32, but there were no phylogenetic differences in primary motor cortex. These findings suggest that, despite the negative correlation between axon length density and brain size observed in our study, the relative innervation density per neuron may vary across species and brain regions.

The results of this study highlight the potential importance of microstructural variation in the evolution of behavioral differences across primate species. Although brain size and neuron numbers have been investigated as predictors of cognitive abilities across species (Herculano-Houzel 2017;

MacLean et al. 2014; Reader and Laland 2002; Shultz and Dunbar 2010), the current study suggests that microstructural variation can provide additional insight into the evolution of cognitive functions. The findings indicate that the microstructure of specific brain regions, such as OFC layers V-VI, may be more closely associated with cognitive abilities such as self-control than overall brain size. This underscores the need to consider both brain size and microstructural variation when investigating the evolution of cognitive functions in primates (Galakhova et al. 2022; Vanderhaeghen and Polleux 2023). Furthermore, the current study emphasizes the importance of examining specific regions beyond large neuroanatomical subdivisions (i.e., whole neocortex) in comparative research on the coevolution of brain and behavior, as different neural systems may have distinct evolutionary trajectories that are associated with different cognitive functions or socioecological adaptations (DeCasien and Higham 2019; Schwartz et al. 2023).

The association between OFC layers V–VI and measures of self-control across primate species may be due to the role of these circuits in inhibitory control, helping to regulate impulsive behavior, and override inappropriate or irrelevant responses. The OFC is involved in monitoring and adjusting actions based on changing circumstances and goals to update behavior (Bechara et al. 2000). Layers V–VI are particularly important for these functions as they receive input from sensory and association areas and send output to other frontal regions that are involved in decision-making and motor planning. In addition, these



layers contain pyramidal neurons that project to subcortical regions, such as the striatum and amygdala, which are involved in reward processing and emotional regulation (Cardinal et al. 2002). The functional significance of OFC layers V–VI in inhibitory control and sensory integration may explain why neuropil fraction in these layers is positively associated with measures of self-control across primate species. Such changes in neuronal connectivity may play a pivotal role in shaping cognitive function and provide a mechanism for species-specific neuroanatomical specialization beyond total cerebral volume or numbers of neurons.

Overall, these findings contribute to our understanding of the evolution and function of the primate frontal cortex and provide a foundation for future research investigating the relationship between microstructure, brain function, and behavior in primates. However, it should be noted that this study has some limitations, including the relatively small sample sizes for some species, and the use of published data for cognitive test performance, which may not be directly comparable across studies. Indeed, self-control is a complex cognitive process that involves both the inhibition in behavioral responses to prepotent stimuli as well as the ability to delay gratification as a means of evaluating the payoff of future rewards (Beran 2018). The two main tasks that MacLean et al. (2014) used were not designed to assess the full range of self-control capabilities. Future studies with larger sample sizes and more standardized cognitive testing protocols may help to clarify these relationships further. In addition, our analysis considered only three frontal regions, which leaves open questions about the evolutionary dynamics and cognitive correlates of other cortical areas. In this regard, it is also worth noting that the parcellation and homologies of the prefrontal cortex across primates continues to be actively debated and revised (Borra et al. 2019; Rapan et al. 2023).

Taken together, our findings suggest that although some microstructure measures are correlated with brain size, they do not necessarily exhibit the same rate of evolution or cognitive correlates. Our study provides a comprehensive view of the microstructural characteristics of primate frontal cortex and highlights the importance of considering the evolutionary and cognitive context when interpreting these characteristics.

**Acknowledgements** We acknowledge Cleveland Metroparks Zoo, Smithsonian National Zoological Park, Milwaukee County Zoo, and the National Chimpanzee Brain Resource (funded by NIH NS092988) for contributing brain specimens used in this study.

Author contributions All authors contributed to the study conception and design. Material preparation, data collection and analysis were performed by Cheryl Stimpson, Jeroen Smaers, and Chet Sherwood. The first draft of the manuscript was written by Cheryl Stimpson, Jeroen Smaers, and Chet Sherwood and all authors commented on previous

versions of the manuscript. All authors read and approved the final manuscript.

**Funding** This research was supported by James S. McDonnell Foundation (220020293), NSF (SMA-1542848, EF-2021785, DRL-2219759), and NIH (AG067419, HG011641).

**Data availability** The dataset generated during the current study is available in Table 1.

### **Declarations**

Conflict of interest The authors have no relevant financial or non-financial interests to disclose. This study utilized human tissue that was procured via the El Paso County coroner's office in Colorado, which provides de-identified samples. Requests for human tissue samples, particularly in biomedical research, are typically processed through the medical examiner or coroner's office, which serves as the legal authority responsible for verifying that all necessary consents and regulations are followed. The George Washington University Research Ethics Committee has confirmed that no ethical approval is required. The protocols are in accordance with the ethical standards of our institution and with the 1964 Helsinki Declaration and its later amendments or comparable ethical standards.

Ethical statement The opinions expressed herein are those of the authors and are not necessarily representative of those of the government of the United States, the Uniformed Services University of the Health Sciences, the Department of Defense (DoD), or the United States Army, Navy or Air Force or the Henry M. Jackson Foundation for the Advancement of Military Medicine, Inc.

### References

Aboitiz F, Garcia VR (1997) The evolutionary origin of the language areas in the human brain. A neuroanatomical perspective. Brain Res Rev 25:381–396

Adams DC (2014) Quantifying and comparing phylogenetic evolutionary rates for shape and other high-dimensional phenotypic data. Syst Biol 63:166–177

Akil M, Lewis DA (1993) The dopaminergic innervation of monkey entorhinal cortex. Cereb Cortex 3(6):533–550

Amiez C, Petrides M (2007) Selective involvement of the middorsolateral prefrontal cortex in the coding of the serial order of visual stimuli in working memory. Proc Nat Acad Sci USA 104(34):13786–13791

Arnold C, Matthews LJ, Nunn CL (2010) The 10k trees website: a new online resource for primate phylogeny. Evol Anthropol 19:114–118

Barbey AK, Koenigs M, Graman J (2013) Dorsolateral prefrontal contributions to human working memory. Cortex 49(5):1195–1205

Bechara A, Damasio H, Damasio AR (2000) Emotion, decision making and the orbitofrontal cortex. Cereb Cortex 10(3):295–307

Benjamini Y, Hochberg Y (1995) Controlling the false discovery rate: a practical and powerful approach to multiple testing. J R Stat Soc Series B Stat Methodol 57:289–300

Beran MJ (2018) Self-Control in Animals and People. Academic Press, London

Berger B, Gaspar P, Verney C (1991) Dopaminergic innervation of the cerebral cortex: unexpected differences between rodents and primates. Trends Neurosci 14(1):21–27

Bianchi S, Stimpson CD, Bauernfeind AL, Schapiro SJ, Baze WB, McArthur MJ, Bronson E, Hopkins WD, Semendeferi K, Jacobs



- B, Hof PR, Sherwood CC (2013) Dendritic morphology of pyramidal neurons in the chimpanzee neocortex: regional specializations and comparison to humans. Cereb Cortex 23(10):2429–2436
- Borra E, Ferroni CG, Gerbella M, Giorgetti V, Mangiaracina C, Rozzi S, Luppino G (2019) Rostro-caudal connectional heterogeneity of the dorsal part of the macaque prefrontal area 46. Cereb Cortex 29(2):485–504
- Butler MA, King AA (2004) Phylogenetic comparative analysis: a modeling approach for adaptive evolution. Am Natural 164:683–695
- Campbell MJ, Morrison JH (1989) Monoclonal antibody to neurofilament protein (SMI-32) labels a subpopulation of pyramidal neurons in the human and monkey neocortex. J Comp Neurol 282:181–205
- Cardinal RN, Parkinson JA, Hall J, Everitt BJ (2002) Emotion and motivation: the role of the amygdala, ventral striatum, and prefrontal cortex. Neurosci Biobehav Rev 26(3):321–352
- Carmichael ST, Price JL (1994) Architectonic subdivision of the orbital and medial prefrontal cortex in the macaque monkey. J Comp Neurol 346:366–402
- Charvet CJ (2023) Mapping human brain pathways: challenges and opportunities in the integration of scales. Brain Behav Evol 98(4):194–209
- Cools R, Arnsten AFT (2022) Neuromodulation of prefrontal cortex cognitive function in primates: the powerful roles of monoamines and acetylcholine. Neuropsychopharmacology 47(1):309–328
- Daubner SC, Le T, Wang S (2011) Tyrosine hydroxylase and regulation of dopamine synthesis. Arch Biochem Biophys 508(1):1–12
- de Lima AD, Voigt T, Morrison JH (1990) Morphology of the cells within the inferior temporal gyrus that project to the prefrontal cortex in the macaque monkey. J Comp Neurol 296:158–172
- Deaner RO, Isler K, Burkart J, van Schaik C (2007) Overall brain size, and not encephalization quotient, best predicts cognitive ability across non-human primates. Brain Behav Evol 70:115–124
- DeCasien AR, Higham JP (2019) Primate mosaic brain evolution reflects selection on sensory and cognitive specialization. Nat Ecol Evol 3(10):1483–1493
- Elston GN, Benavides-Piccione R, Elston A, Manger PR, DeFelipe J (2011) Pyramidal cells in prefrontal cortex of primates: marked differences in neuronal structure among species. J Front Neuroanat 5(2):1–17
- Fishell G, Kepecs A (2020) Interneuron types as attractors and controllers. Annu Rev Neurosci 8(43):1–30
- Folloni D, Sallet J, Khrapitchev AA, Sibson N, Verhagen L, Mars RG (2019) Dichotomous organization of amygdala/temporal-prefrontal bundles in both humans and monkeys. Elife 8:e47175
- Frey S, Zlatkina V, Petrides M (2009) Encoding touch and the orbitofrontal cortex. Hum Brain Mapp 30:650–659
- Gabbott PLA, Bacon SJ (1996) Local circuit neurons in the medial prefrontal cortex (areas 24a, b, c, 25 and 32) in the monkey: II. Quantitative areal and laminar distributions. J Comp Neurol 364:609–636
- Gabbott PLA, Dickie BGM, Vail RR, Headlam AJN, Bacon SJ (1997) Local-circuit neurons in the medial prefrontal cortex (areas 25, 32, 24b) in the rat: morphology and quantitative distribution. J Comp Neurol 377:465–499
- Galakhova AA, Hunt S, Wilbers R, Heyer DB, de Kock CPJ, Mansvelder HD, Goriounova NA (2022) Evolution of cortical neurons supporting human cognition. Trends Cogn Sci 26(11):909–922
- Gaspar P, Berger B, Febvret A, Vigny A, Henry JP (1989) Catecholamine innervation of the human cerebral cortex as revealed by comparative immunohistochemistry of tyrosine hydroxylase and dopamine-beta-hydroxylase. J Comp Neurol 279(2):249–271
- Ghashghaei HT, Hilgetag CC, Barbas H (2007) Sequence of information processing for emotions based on the anatomic dialogue between prefrontal cortex and amygdala. Neuroimage 34(3):905–923

- Goldman-Rakic PC (1988) Topography of cognition: parallel distributed networks in primate association cortex. Ann Rev Neurosci
- Gundersen HJ (1988) The nucleator. J Microsc 151(Pt 1):3-21
- Herculano-Houzel S (2017) Numbers of neurons as biological correlates of cognitive capability. Curr Opin Behav Sci 16:1–7
- Herculano-Houzel S, Collins CE, Wong P, Kaas JH (2007) Cellular scaling rules for primate brains. Proc Natl Acad Sci USA 104(9):3562–3567
- Hilgetag CC, Beul SF, van Albada SJ, Goulas A (2019) An architectonic type principle integrates macroscopic cortico-cortical connections with intrinsic cortical circuits of the primate brain. Netw Neurosci 3(4):905–923
- Hof PR, Sherwood CC (2005) Morphomolecular neuronal phenotypes in the neocortex reflect phylogenetic relationships among certain mammalian orders. Anat Rec Part A 287:1153–1163
- Hof PR, Mufson EJ, Morrison JH (1995a) Human orbitofrontal cortex: cytoarchitecture and quantitative immohistochemical parcellation. J Comp Neurol 359:48–68
- Hof PR, Nimchinsky EA, Morrison JH (1995b) Neurochemical phenotype of corticocortical connections in the macaque monkey: quantitative analysis of a subset of neurofilament protein-immunoreactive projection neurons in frontal, parietal, temporal and cingulate cortex. J Comp Neurol 362:109–133
- Issa HA, Staes N, Diggs-Galligan S, Stimpson CD, Gendron-Fitzpatrick A, Taglialatela JP, Hof PR, Hopkins WD, Sherwood CC (2019) Comparison of bonobo and chimpanzee brain microstructure reveals differences in socio-emotional circuits. Brain Str Funct 224(1):239–251
- Jacobs B, Schall M, Prather M, Kapler E, Driscoll L, Baca S, Jacobs J, Ford K, Wainwright M, Treml M (2001) Regional dendritic and spine variation in human cerebral cortex: a quantitative Golgi study. Cereb Cortex 11:558–571
- Jacobs B, Lubs J, Hannan M, Anderson K, Butti C, Sherwood CC, Hof PR, Manger PR (2011) Neuronal morphology in the African elephant (*Loxodonta africana*) neocortex. Brain Str Funct 215:273–298
- Jacobs B, Garcia ME, Shea-Shumsky NB, Tennison ME, Schall M, Saviano MS, Tummino TA, Bull AJ, Driscoll LL, Raghanti MA, Lewandowski AH, Wicinski B, Ki Chui H, Bertelsen MF, Walsh T, Bhagwandin A, Spocter MA, Hof PR, Sherwood CC, Manger PR (2018) Comparative morphology of gigantopyramidal neurons in primary motor cortex across mammals. J Comp Neurol 526(3):496–536
- Kass JH (2013) The evolution of brains from early mammals to humans. Rev Cog Sci 4(1):33–45
- Khabbazian M, Kriebel R, Rohe K, Ané C (2016) Fast and accurate detection of evolutionary shifts in Ornstein-Uhlenbeck models. Methods Ecol Evol 7:811–824
- MacLean EL, Hare B, Nunn CL, Addessi E, Amici F, Anderson RC, Aureli F, Baker JM, Bania AE, Barnard AM, Boogert NJ, Brannon EM, Bray EE, Bray J, Brent LJ, Burkart JM, Call J, Cantlon JF, Cheke LG, Clayton NS, Delgado MM, DiVincenti LJ, Fujita K, Herrmann E, Hiramatsu C, Jacobs LF, Jordan KE, Laude JR, Leimgruber KL, Messer EJ, Moura AC, Ostojić L, Picard A, Platt ML, Plotnik JM, Range F, Reader SM, Reddy RB, Sandel AA, Santos LR, Schumann K, Seed AM, Sewall KB, Shaw RC, Slocombe KE, Su Y, Takimoto A, Tan J, Tao R, van Schaik CP, Virányi Z, Visalberghi E, Wade JC, Watanabe A, Widness J, Young JK, Zentall TR, Zhao Y (2014) The evolution of self-control. Proc Natl Acad Sci USA 111(20):E2140–E2148
- Mai JK, Paxinos G, Voss T (2007) Atlas of the Human Brain, 3rd edn. Academic Press, Amsterdam
- Pagel M (1999) Inferring the historical patterns of biological evolution. Nature 401:877–884



- Passingham RE, Lau H (2022) Do we understand the prefrontal cortex? Brain Str Funct 228(5):1095–1105
- Passingham RE, Wise SP (2012) The Neurobiology of the Prefrontal Cortex. Oxford University Press, Oxford
- Paxinos G, Petrides M, Huang X, Toga AW (2008) The Rhesus Monkey Brain in Stereotaxic Coordinates, 2nd edn. Academic Press, Amsterdam
- Paxinos G, Watson C, Petrides M, Rosa M, Tokuno H (2011) The Marmoset Brain in Stereotaxic Coordinates, 1st edn. Academic Press. Amsterdam
- Petrides M (1991) Functional specialization within the dorsolateral frontal cortex for serial order memory. Proc R Soc Lond B 246:299–306
- Petrides M, Alivistos B, Mayer E, Evans AC (1993) Functional activation of the human frontal cortex during the performance of verbal working memory tasks. Proc Natl Acad Sci USA 90:878–882
- Preuss TM, Goldman-Rakic PS (1991) Myelo- and cytoarchitechture of the granular frontal cortex and surrounding regions in the strepsirhine primate *Galago* and the anthropoid primate *Macaca*. J Comp Neurol 310:429–474
- Preuss TM, Wise SP (2022) Evolution of prefrontal cortex. Neuropsychopharmacology 47(1):3–19
- Provost J, Petrides M, Monchi O (2010) Dissociating the role of the caudate nucleus and dorsolateral prefrontal cortex in the monitoring of events within human working memory. Eur J Neurosci 32:873–880
- Raghanti MA, Stimpson CD, Marcinkiewicz JL, Erwin JM, Hof PR, Sherwood CC (2008a) Differences in cortical serotonergic innervation among humans, chimpanzees and macaque monkeys: a comparative study. Cereb Cortex 18(3):584–597
- Raghanti MA, Stimpson CD, Marcinkiewicz JL, Erwin JM, Hof PR, Sherwood CC (2008b) Cortical dopaminergic innervation among human, chimpanzees, and macaque monkeys: a comparative study. Neuroscience 155(1):203–220
- Raghanti MA, Spocter MA, Stimpson CD, Erwin JM, Bonar CJ, Allman JM, Hof PR, Sherwood CC (2009) Species-specific distributions of tyrosine hydroxylase-immunoreactive neurons in the prefrontal cortex of anthropoid primates. Neuroscience 158:1551–1559
- Rapan L, Froudist-Walsh S, Niu M, Xu T, Zhao L, Funck T, Wang XJ, Amunts K, Palomero-Gallagher N (2023) Cytoarchitectonic, receptor distribution and functional connectivity analyses of the macaque frontal lobe. Elife 12:e82850
- Rash BG, Arellano JI, Duque A, Rakic P (2023) Role of intracortical neuropil growth in the gyrification of the primate cerebral cortex. Proc Natl Acad Sci USA 120(1):e2210967120
- Reader SM, Laland KN (2002) Social intelligence, innovation, and enhanced brain size in primates. Proc Natl Acad Sci USA 99(7):4436–4441
- Rohlf FJ (2001) Comparative methods for the analysis of continuous variables: geometric interpretations. Evolution 55:2143–2160
- Rolls ET (2004) The functions of the orbitofrontal cortex. Brain Cogn 55(1):11-29
- Sallet J, Mars RB, Noonan MP, Neubert F, Jbabdi S, O'Reilly JX, Filippini N, Thomas AG, Rushworth MF (2013) The organization of dorsal frontal cortex in humans and macaques. J Neurosci 33(30):12255–12274
- Sara SJ, Bouret S (2012) Orienting and reorienting: the locus coeruleus mediates cognition through arousal. Neuron 76(1):130-141
- Schwartz E, Nenning KH, Heuer K, Jeffery N, Bertrand OC, Toro R, Kasprian G, Prayer D, Langs G (2023) Evolution of cortical geometry and its link to function, behaviour and ecology. Nat Commun 14(1):2252

- Semendeferi K, Armstrong E, Schleicher A, Zilles K, van Hoesen GW (1998) Limbic frontal cortex in hominoids: a comparative study of area 13. Am J Phys Anthropol 106:129–155
- Semendeferi K, Teffer K, Buxhoeveden DP, Park MS, Blusau S, Amunts K, Travis K, Buckwalter J (2011) Spatial organization of neurons in the frontal pole sets humans apart from great apes. Cereb Cortex 21(7):11485–11497
- Sharma Y, Xu T, Graf WM, Fobbs A, Sherwood CC, Hof PR, Allman JM, Manaye KF (2010) Comparative anatomy of the locus coeruleus in humans and nonhuman primates. J Comp Neurol 518(7):963–971
- Sherwood CC, Lee PWH, Rivara C, Holloway RL, Gilissen EPE, Simmons RMT, Hakeem A, Allman JM, Erwin JM, Hof PR (2003) Evolution of specialized pyramidal neurons in primate visual and motor cortex. Brain Behav Evol 61:28–44
- Sherwood CC, Holloway RL, Erwin JM, Hof PR (2004) Cortical orofacial motor representation in Old World monkeys, great apes, and humans. II. Stereologic analysis of chemoarchitecture. Brain Behav Evol 63(2):82–106
- Sherwood CC, Raghanti MA, Stimpson CD, Donar CJ, de Sousa AA, Preuss TM, Hof PR (2007) Scaling of inhibitory interneurons in areas V1 and V2 of anthropoid primates as revealed by calcium-binding protein immunohistochemistry. Brain Behav Evol 69:176–195
- Sherwood CC, Miller SB, Karl M, Stimpson CD, Phillips KA, Jacobs B, Hof PR, Raghanti MA, Smaers JB (2020) Invariant synapse density and neuronal connectivity scaling in primate neocortical evolution. Cereb Cortex 30(10):5604–5615
- Shi Y, Wang M, Mi D, Lu T, Wang B, Dong H, Zhong S, Chen Y, Sun L, Zhou X, Ma Q, Liu Z, Wang W, Zhang J, Wu Q, Marín O, Wang X (2021) Mouse and human share conserved transcriptional programs for interneuron development. Science 374(6573):eabj6641
- Shu SY, Ju G, Fan LZ (1988) The glucose oxidase-DAB-nickel method in peroxidase histochemistry of the nervous system. Neurosci Lett 85:169–171
- Shultz S, Dunbar RIM (2010) Species differences in executive function correlate with hippocampus volume and neocortex ratio across nonhuman primates. J Comp Psychol 123(3):252–260
- Smaers JB, Gómez-Robles A, Parks AN, Sherwood CC (2017) Exceptional evolutionary expansion of prefrontal cortex in great apes and humans. Curr Biol 27:714–720
- Spocter MA, Hopkins WD, Barks SK, Bianchi S, Hehmeyer AE, Anderson SM, Stimpson CD, Fobbs AJ, Hof PR, Sherwood CC (2012) Neuropil distribution in the cerebral cortex differs between humans and chimpanzees. J Comp Neurol 520:2917–2929
- Stimpson CD, Barger N, Taglialatela JP, Gendron-Fitzpatrick A, Hof PR, Hopkins WD, Sherwood CC (2016) Differential serotonergic innervation of the amygdala in bonobos and chimpanzees. Soc Cogn Affect Neurosci 11:413–422
- Tacutu R, Thornton D, Johnson E, Budovsky A, Barardo D, Craig T, Diana E, Lehmann G, Toren D, Wang J, Fraifeld VE, de Magalhães JP (2018) Human Ageing Genomic Resources: new and updated databases. Nucleic Acids Res 46(D1):D1083–D1090
- Van der Gucht E, Vandesande F, Arckens L (2001) Neurofilament protein: a selective marker for the architectonic parcellation of the visual cortex in adult cat brain. J Comp Neurol 441(4):345–368
- Vanderhaeghen P, Polleux F (2023) Developmental mechanisms underlying the evolution of human cortical circuits. Nat Rev Neurosci 24(4):213–232
- Wallis JD, Dias R, Robbins TW, Roberts AC (2001) Dissociable contributions of the orbitofrontal and lateral prefrontal cortex of the marmoset to performance on a detour reaching task. Eur J Neurosci 13(9):1797–1808



Wendland JR, Lesch KP, Newman TK, Timme A, Gachot-Neveu H, Thierry B, Suomi SJ (2005) Differential functional variability of serotonin transporter and monoamine oxidase A genes in the macaque species displaying contrasting levels of aggressionrelated behavior. Behav Genet 36(2):163–172

**Publisher's Note** Springer Nature remains neutral with regard to jurisdictional claims in published maps and institutional affiliations.

Springer Nature or its licensor (e.g. a society or other partner) holds exclusive rights to this article under a publishing agreement with the author(s) or other rightsholder(s); author self-archiving of the accepted manuscript version of this article is solely governed by the terms of such publishing agreement and applicable law.

